Universal Scaling Theory of the Boundary Geometric Tensor in Disordered Metals

Miklós Antal Werner,[1] Arne Brataas,[2] Felix von Oppen,[3] and Gergely Zaránd[1]

[1] *Exotic Quantum Phases "Momentum" Research Group, Department of Theoretical Physics, Budapest University of Technology and Economics, 1111 Budapest, Budafoki út 8, Hungary*

[2] *Center for Quantum Spintronics, Department of Physics, Norwegian University of Science and Technology, NO-7491 Trondheim, Norway*

[3] *Dahlem Center for Complex Quantum Systems and Fachbereich Physik, Freie Universität Berlin, 14195 Berlin, Germany*

(Dated: July 20, 2018)

We investigate the finite-size scaling of the boundary quantum geometric tensor (QGT) numerically close to the Anderson localization transition in the presence of small external magnetic fields. The QGT exhibits universal scaling and reveals the crossover between the orthogonal and unitary critical states in weak random magnetic fields. The flow of the QGT near the critical points determines the critical exponents. Critical distributions of the QGT are universal and exhibit a remarkable isotropy even in a homogeneous magnetic field. We predict universal and isotropic Hall conductance fluctuations at the metal-insulator transition in an external magnetic field.

PACS numbers: 72.15.Rn, 73.20.Fz, 05.10.Cc, 05.30.Rt

Introduction.— The geometrical structure of the Hilbert space continues to receive a lot of attention. The Fubini-Study metric tensor of the Hilbert space [1, 2], also referred to as Fisher information metric [2], provides a natural measure of distance in the Hilbert space, related to quantum fidelity – a fundamental concept in quantum information science [3]. The Fubini-Study metric tensor [4, 5] has also been used to analyze quantum critical points in many systems including interacting spin models [6, 7], many-body systems [8, 9], and systems exhibiting topological order [10, 11]. Non-adiabatic dynamics in driven quantum systems is also deeply connected to the Riemannian metric of the ground state manifold [12].

Another fundamental geometric concept in quantum theory is the Berry phase [13], a geometric invariant in quantum state manifolds. The presence of a non-trivial Berry curvature leads to interesting quantum interference phenomena [14, 15] and impacts the trajectory of wave packets [16, 17]. The Zak phase [15, 18] – the Berry-phase associated with closed loops in the Brillouin zone – and its higher dimensional analogues play central role in the description of topological insulators [19–21]. Non-abelian Berry phases of degenerate ground state manifolds, on the other hand [22], can generate spin relaxation in the absence of external magnetic fields [23] and underlie realizations of non-abelian statistics in topological superconductors [24].

The concepts of the Fubini-Study metric tensor and the Berry phase can be unified through the so-called quantum geometric tensor (QGT) [25]. Consider a quantum system, whose Hamiltonian $H(\{\phi_i\})$ and eigenstates $|\alpha(\{\phi_i\})\rangle$ depend smoothly on a set of real parameters, ϕ_i. The QGT of the eigenstate $|\alpha(\{\phi_i\})\rangle$ at a point $\{\phi_i\}$ in the parameter space is then defined as

$$Q^{ij}_{\alpha}(\phi) \equiv \langle \partial_{\phi_i}\alpha \left| \partial_{\phi_j}\alpha \right\rangle - \langle \partial_{\phi_i}\alpha \left| \alpha \right\rangle \langle \alpha \left| \partial_{\phi_j}\alpha \right\rangle \ . \qquad (1)$$

The matrix Q^{ij}_{α} is Hermitian and gauge invariant. Its (symmetric) real part is the metric tensor associated with the manifold $|\alpha(\phi)\rangle$ [1, 25], while its imaginary (antisymmetric) part is the Berry curvature form [13, 25], whose surface integral yields the Berry phase associated with closed loops in parameter space.

In the present work, we demonstrate that the QGT offers deep insight into a long-standing problem in condensed matter physics, Anderson's disorder-driven metal-insulator (MI) transition in small external magnetic fields [26, 27]. In particular, the structure of the QGT reflects the universality class of the Anderson transition. Elements of the QGT display universal finite size scaling close to the metal-insulator transition, and capture the flow between the orthogonal ($B = 0$) and unitary ($B \neq 0$) universality classes. At the transition, the elements of the QGT have universal distributions, characteristic of the underlying symmetry of the transition, but, surprisingly, independent of the direction of the external field. We predict that these universal fluctuations show up as universal and isotropic Hall conductance fluctuations at the metal-insulator transition.

Mathematical model.— To investigate the effect of small magnetic fields on the properties of eigenstates close to the MI transition, we study disordered non-interacting spinless fermions on a three-dimensional cubic lattice in external magnetic fields, described by the Hamiltonian

$$\hat{H} = \sum_{\mathbf{r}} V_{\mathbf{r}} c^{\dagger}_{\mathbf{r}} c_{\mathbf{r}} - \sum_{\langle \mathbf{r},\mathbf{r}' \rangle} \left(t_{\mathbf{r}\mathbf{r}'} c^{\dagger}_{\mathbf{r}} c_{\mathbf{r}'} + H.c. \right) \ . \qquad (2)$$

Here $c^{\dagger}_{\mathbf{r}}$ ($c_{\mathbf{r}}$) creates (annihilates) a fermion on site $\mathbf{r} = (x, y, z)$, and the $V_{\mathbf{r}}$ denote independent random variables uniformly distributed in the interval $[-W/2, W/2]$. The second term in Eq. (2) accounts for nearest neighbor hopping, with the magnetic field incorporated through the Peierls substitution, $t_{\mathbf{r}\mathbf{r}'} = t\, e^{i2\pi A_{\mathbf{r}\mathbf{r}'}}$. In homogeneous fields we use the gauge of Ref. 28 for the bond vector po-

tentials $A_{\mathbf{r}\mathbf{r}'}$, while in random fields the $A_{\mathbf{r}\mathbf{r}'}$ denote independent, uniformly distributed random variables from the interval $[-W_B/2, W_B/2]$.

Single particle eigenstates of $\hat{H}$ are usually classified as 'extended' or 'localized'. The latter emerge close to the band edge, and are separated from the former at small disorder by so-called mobility edges [27]. Correspondingly, the system is insulating or metallic if states at the Fermi energy are localized or extended, respectively.

Universality classes and criticality.— The spatial structure of localized (extended) states is characterized by the localization (coherence) length, ξ. These latter length scales depend on the energy of the states, and diverge at the mobility edge E_c following a power law, $\xi \sim |E - E_c|^{-\nu}$. This divergent behavior is the ultimate basis of single parameter scaling theory [29]: assuming that close to the MI transition ξ is the only relevant length scale, the zero temperature dimensionless conductance $g = G/(e^2/h)$ of a system of size L must be a function of L/ξ only, and therefore must obey the scaling equation, $\partial g/\partial \ln L = \beta(g)$, with $\beta(g)$ a universal function. This beta function has indeed been determined both perturbatively and numerically in the absence of external magnetic field. Its universal properties have been convincingly demonstrated [29–31]. In the presence of a sufficiently strong time reversal breaking, however, a clearly distinct, but apparently also universal scaling has been observed [32].

The beautiful construction of single parameter scaling must therefore necessarily break down in small magnetic fields. A weak external magnetic field generates a magnetic length scale, L_B, which is typically much larger than all microscopic length scales. As a consequence, the dimensionless conductance should also depend on the ratio L_B/ξ, implying a two-parameter dependence, $g = g(L/\xi, L_B/\xi)$, and invalidating the single parameter scaling theory [33]. Fortunately, very close to the transition — or in very large fields — we have $L_B/\xi \to 0$. Therefore universal scaling is still recovered at criticality, but with a modified 'unitary' beta function, $\beta \to \tilde{\beta}(g)$ [34]. So far the intriguing cross-over between orthogonal and unitary criticality has not been observed systematically in experiments, but it has been investigated to some extent within the non-linear sigma model approach [35, 36], where the cross-over in a weak magnetic field has been addressed near the orthogonal critical point in $2 + \varepsilon$ dimensions. Perturbative scaling gives a qualitative picture of the cross-over, but the approximate values of the critical exponents are in significant disagreement with numerical results [31]. A precise description of criticality near the unitary fixed point therefore appears to be beyond the reach of this perturbative approach. Orthogonal-unitary cross-over has been observed numerically in the critical level spacing statistics in Ref. 37, but the violation of the one parameter scaling theory is not addressed in that work. As we show now, the quantum geometric tensor provides an ideal tool to characterize this cross-over.

Two-parameter QGT scaling theory.— In the spirit of Thouless [2], who related the boundary condition dependence of single particle energies to the dimensionless conductance, we shall investigate the boundary condition dependence of the single particle eigenstates of Eq. (2), determined by the eigenvalue equation

$$|\alpha\rangle = \sum_{\mathbf{r}} \alpha(\mathbf{r}) c^\dagger_{\mathbf{r}} |0\rangle \ , \quad \hat{H}\,|\alpha\rangle = E_\alpha\,|\alpha\rangle \ . \tag{3}$$

We prescribe here twisted boundary conditions, $\alpha_\phi(\mathbf{r} + L\,\mathbf{n}) = e^{i\,\mathbf{n}\cdot\phi}\alpha_\phi(\mathbf{r})$, with $\mathbf{n} = \{n_x, n_y, n_z\}$ a vector of arbitrary integers, and $\phi = \{\phi_x, \phi_y, \phi_z\}$ collecting the boundary twists into a single vector. For a given system size and disorder realization, we can now view each eigenstate as a manifold, $|\alpha\rangle = |\alpha(\phi)\rangle$, and define the corresponding QGT at zero twist, $Q^{ij}_\alpha \equiv Q^{ij}_\alpha(\phi = 0)$. In the presence of time reversal symmetry, the antisymmetric part of the tensor Q^{ij}_α vanishes. Moreover, the sum of Q^{ij}_α over occupied states is the Hall conductance [39]. The antisymmetric part of the QGT is therefore a promising dimensionless indicator of time reversal symmetry breaking, while the diagonal elements of Q^{ij} are reminiscent of the Thouless number, and turn out to be in one to one correspondence with it [40].

These observations lead us to introducing two real parameters for each eigenstate $|\alpha\rangle$,

$$g(\alpha) \equiv \mathrm{tr}\{Q^{ij}_\alpha\}\,, \quad h(\alpha) \equiv i\,(Q^{xy}_\alpha - Q^{yx}_\alpha) \ . \tag{4}$$

These parameters fluctuate strongly for distinct disorder potentials and eigenstates. We therefore consider their *typical* magnitude, averaged over a large ensemble of samples,

$$\ln g_{\rm typ} \equiv \overline{\ln|g(\alpha)|}_{E_\alpha \approx E}, \quad \ln h_{\rm typ} \equiv \overline{\ln|h(\alpha)|}_{E_\alpha \approx E}, \tag{5}$$

that are functions of energy, system size, disorder strength, and magnetic field. As we demonstrate, these quantities behave as good scaling parameters, and satisfy the universal scaling equations

$$\frac{\partial g_{\rm typ}}{\partial \log L} = \beta_g(g_{\rm typ}, h_{\rm typ}) \ , \ \frac{\partial h_{\rm typ}}{\partial \log L} = \beta_h(g_{\rm typ}, h_{\rm typ}) \ . \tag{6}$$

The content of Eq. (6) is that the logarithmic size dependence of the typical values $g_{\rm typ}$ and $h_{\rm typ}$ is completely independent of microscopic details such as W, W_B, or the location of the Fermi energy, and is solely determined by $g_{\rm typ}$ and $h_{\rm typ}$.

To verify the scaling hypothesis of Eq. (6), we first performed finite size computations in a homogeneous field, and evaluated the logarithmic derivatives on the left hand side for various disorder realizations and energies numerically. In the absence of external field, $h(\alpha) \equiv 0$ for each level, we recover a flow along the axis $h_{\rm typ} = 0$

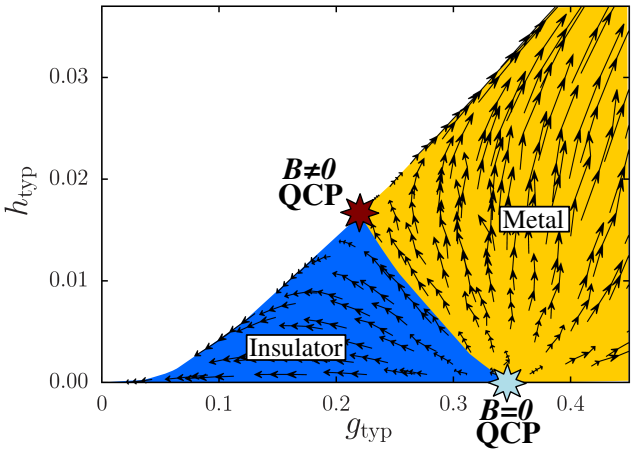

FIG. 1. *(Color online)* Finite size scaling of $g_{\rm typ}$ and $h_{\rm typ}$ in a random magnetic field. Arrows indicate the direction of the renormalization group flow upon increasing the the system size from $L = 8$ to $L = 14$. The $B = 0$ (orthogonal) and $B \neq 0$ (unitary) quantum critical points are denoted by light and red stars, respectively. The blue region indicates the insulating phase, while the metallic phase is yellow.

of the $(g_{\rm typ}, h_{\rm typ})$ plane, as shown in Fig. 1. This flow is governed by the one-parameter function, $\beta_g(g_{\rm typ}, 0)$, which we determined numerically (see Ref. [40] for details). A critical point emerges at $g^*_{B=0} = 0.3309(18)$, and the numerically determined β-function yields a critical exponent $\nu_{B=0} = 1.560(63)$, in good agreement with the best known result for orthogonal systems, $\nu_{\rm orth} = 1.571(8)$ [31]. We thus find that the *trace* of the QGT, $\sim g$, behaves as an appropriate scaling variable, which can be used to replace the dimensionless conductance of the single-parameter scaling theory of Ref. 29 – or the Thouless conductance [2].

Piercing just *one* flux quantum through our system brings us immediately to the unitary class of systems: It yields another, universal one-parameter trajectory in the $(g_{\rm typ}, h_{\rm typ})$ plane, with a critical point at $g^*_{B\neq 0} = 0.22215(87)$ and a finite $h^*_{B\neq 0} = 0.01683(13)$. Again, the extracted value of the critical exponent, $\nu_{B\neq 0} = 1.459(64)$ agrees well with the most accurate estimate in the literature, $\nu_{\rm unitary} = 1.424(15)$ [41]. These results prove that the antisymmetric part h of the QGT provides a good dimensionless, universal variable to distinguish the orthogonal and unitary universality classes.

Unfortunately, within the torus geometry used here, we cannot pierce less than one flux quantum through the system [28], and this is already too large to observe the flow between the two critical points in the $(g_{\rm typ}, h_{\rm typ})$ plane. We circumvented this difficulty by applying *random* vector potentials. In this case, we can tune the strength of time reversal symmetry breaking continuously by changing the strength W_B of the random vector potentials. Reassuringly, in large random fields, $W_B \gtrsim 0.15$, the flow perfectly coincides with the one parameter trajectory that we observed in homogeneous fields. In small random fields ($W_B \lesssim 0.15$), however, we can now clearly observe a two-parameter flow crossing over between the $B = 0$ and $B \neq 0$ universality classes, as presented in Fig. 1. We should emphasize that the flow in Fig. 1 is independent of microscopic details, and is generated at each point by collecting data at different energies, and for different values of the disorder parameters W and W_B. A detailed analysis of the flow around the fixed points also allows us to extract the scaling exponents associated with the relevant (and leading irrelevant) operator [42] at the orthogonal (unitary) fixed points, associated with time reversal symmetry breaking,

$$y_{B=0} = 0.990(11), \quad y_{B\neq 0} = -2.12(23).$$

Critical QGT distributions.— The typical values $g_{\rm typ}$ and $h_{\rm typ}$ still allow for large sample to sample and level to level fluctuations of $g(\alpha)$ and $h(\alpha)$ at and around the Fermi energy, and a corresponding broad distribution. At the critical points $(g^*_{\rm typ}, h^*_{\rm typ})$, the Fermi energy lies just on the mobility edge, E_C, where these distributions are expected to become independent of the sample size (scale invariant) and universal. To determine these universal distributions, we first have to locate the mobility edge for each disorder strength W and W_B, and extract the critical distributions of the quantum geometric tensor Q^{ij}_α in its neighborhood.

Fig. 2 summarizes the results for the unitary ($B \neq 0$) critical point. (For distributions at the $B = 0$ orthogonal critical point see Fig. S3 of the Supplemental Material [40].) The critical distributions of $g(\alpha)$ and $h(\alpha)$ are indeed independent of system size, disorder, and magnetic field strength. The power law tail of the distribution of $g(\alpha)$ resembles that of the critical distribution of the Thouless curvature [43], though the exponent of the power law is found to be different: while, in agreement with heuristic arguments presented in the Supplemental Material [40], $P(g)$ falls off with a power close to 2.5, the exponent of the Thouless curvature's distribution is around 4 [44, 45]. Interestingly, systems with homogeneous and random fields give rise to identical distributions. This surprising agreement of the distributions in homogeneous and random fields indicates that the *direction* of the magnetic field is *irrelevant* at the critical point, at least from the point of view of the quantum geometric tensor's structure and distribution. Therefore the statistics of the QGT should be not only universal, but also rotationally invariant at the critical point.

To explore this symmetry, we generalized the parameter h and characterized the antisymmetric part of Q^{ij} by three independent real numbers forming an axial vector,

$$h_k(\alpha) \equiv i \sum_{i,j} \epsilon_{kij}\, Q^{ij}_\alpha \,, \tag{7}$$

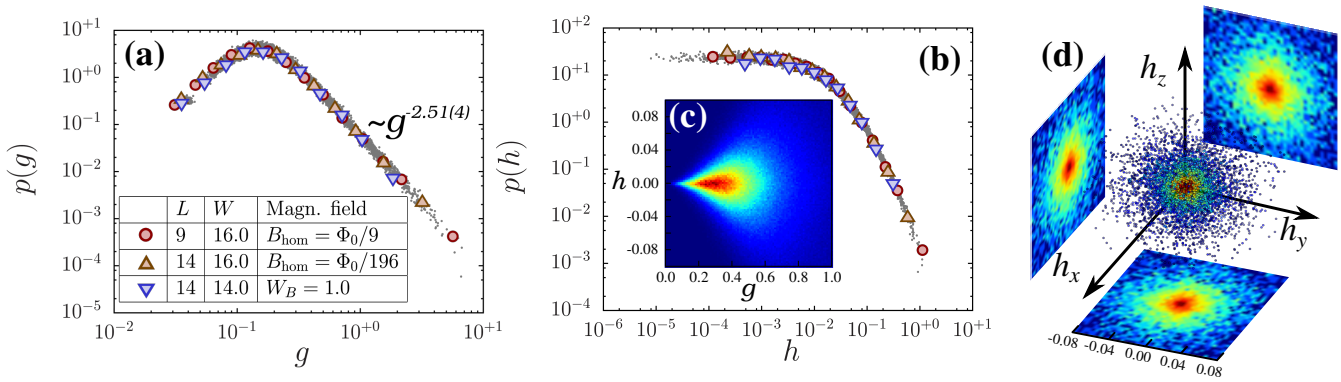

FIG. 2. *(Color online)* **(a)** Probability density function of g at the unitary ($B \neq 0$) critical point. Distributions were extracted from systems of different system sizes, magnetic fields, and disorder strengths, with the energy at the mobility edge. Different symbols refer to data extracted from systems with different system sizes, disorder strengths, and homogeneous or random field strengths, as specified in the legend. The cloud of small gray dots shows the distribution of g, obtained by merging all data of all parameter sets. **(b)** The $h > 0$ part of the probability density function of the parameter h at the unitary ($B \neq 0$) critical point. Symbols correspond to the parameter sets as in the panel (a), while small gray dots show the merged distribution. **(c)** Joint distribution of g and h at the unitary critical point. **(d)** Joint critical distribution of the parameters h_k, characterizing the antisymmetric part of the QGT, determined at the unitary fixed point. Points in the three-dimensional cloud represent individual eigenstates, computed in a homogeneous magnetic field $B = \Phi_0/9$ along the z direction, in a system of size $L = 9$ and disorder $W = 17$. The almost perfect rotational symmetry of the distribution is supported by the two-dimensional marginals shown on planes next to the cloud.

with ϵ_{kij} the completely antisymmetric tensor. As shown in Fig. 2.d, the joint critical distribution of the three parameters $h_{x,y,z}$ shows remarkable isotropy, even in a strong homogeneous magnetic field and the typical values of $|h_{x,y,z}|$ are all equal. This observation also justifies *a posteriori* the somewhat arbitrary choice of $h = h_z$ as a scaling variable in a random field, too.

A detailed analysis of the distribution of the h_i, shown in Fig. 2.d – as well as that of the real symmetrical components of the QGT, shown in the Supplemental Material – reveals that the distribution of the QGT is not perfectly O(3) symmetrical, and slightly breaks rotational symmetry down to a cubic symmetry even at the critical point. This small symmetry breaking is equally present in random and homogeneous fields, therefore it cannot be induced by the direction of the magnetic field [40], which could anyway only explain the emergence of a tetragonal symmetry. Rather, we explain this behavior as an effect of the cubic shape of the system on the structure of critical wave functions.

Universal Hall conductance fluctuations.— The behavior of the QGT at the critical point has an interesting experimental consequence. The antisymmetric part of the QGT is directly related to the Hall conductance through the Kubo-Greenwood formula [39, 46],

$$G_H^k = \frac{e^2}{\hbar} \sum_{E_\alpha < E_F} h_k(\alpha) \; . \tag{8}$$

with E_F the Fermi-energy, and $k \in \{x, y, z\}$ the direction perpendicular to the plane of the Hall measurement. According to Eq. (8), chemical potential changes in a coherent mesoscopic sample induce *Hall conductance fluctuations*, determined by the critical distribution of the QGT. Consequently, in a magnetic field, at the metal-insulator transition, we predict the emergence of universal and isotropic Hall conductance fluctuations in a mesoscopic sample. These fluctuations as well as their precise distributions should be accessible in present-day experiments. As a possible implementation, one can think of disordered metallic samples in a Hall-measurement setup, with the mobility edge tuned, e.g., by applying strain. Changing the external magnetic field or the application of back gates should generate the mesoscopic fluctuations discussed here.

Conclusions.— In this work, we demonstrated that the QGT provides a unified framework to capture the cross-over between the orthogonal and unitary Anderson-localized critical states. Our results show that the geometrical structure of the eigenstates is intimately connected to their spatial structure and the conductance properties at the Fermi energy. A natural generalization would be to study the behavior of QGT in models with weak spin-orbit coupling [41, 47]. In that case – in the presence of time reversal symmetry – one expects a two parameter crossover between the orthogonal and the symplectic classes. If both spin-orbit coupling and magnetic fields are present, an even more complicated, three parameter behavior may appear. It is an intriguing question if the related cross-overs are reflected in the geometrical structure of the eigenstates, and if the expected three parameter scaling can be captured by the QGT. Generalizations in the presence of interaction and for the

many body localization (MBL) transition are other open lines of research [48, 49], though the extremely limited system sizes, make the scaling analysis of the QGT at the MBL transition a significantly harder task.

Acknowledgement.— We are grateful to Nigel Cooper and Bert Halperin for illuminating discussions. This research has been supported by the Hungarian National Research, Development and Innovation Office (NKFIH) through Grant Nos. SNN118028 and the Hungarian Quantum Technology National Excellence Program (Project No. 2017-1.2.1-NKP-2017- 00001). M.A.W has also been supported by the ÚNKP-17-3-IV New National Excellence Program of the Ministry of Human Capacities.

[1] J. P. Provost and G. Vallee, Comm. Math. Phys. **76,** 289-301 (1980).
[2] R. A. Fisher, Proc. Cambridge Philos. Soc. **22,** 700 (1925).
[3] M. A. Nielsen and I. L. Chuang, *Quantum Computation and Quantum Information* (Cambridge University Press, 2000), p. 403-416.
[4] P. Zanardi, P. Giorda, and M. Cozzini, Phys. Rev. Lett. **99,** 100603 (2007).
[5] M. Kolodrubetz, V. Gritsev, and A. Polkovnikov Phys. Rev. B **88,** 064304 (2013).
[6] P. Zanardi and N. Paunkovic, Phys. Rev. E **74,** 031123 (2006).
[7] S. Garnerone, N. T. Jacobson, S. Haas, and P. Zanardi, Phys. Rev. Lett. **102,** 057205 (2009).
[8] P. Buonsante and A. Vezzani, Phys. Rev. Lett. **98,** 110601 (2007).
[9] J. Carrasquilla, S. R. Manmana, and M. Rigol, Phys. Rev. A **87,** 043606 (2013).
[10] S. Yang, S.-J. Gu, C.-P. Sun, and H.-Q. Lin, Phys. Rev. A **78,** 012304 (2008).
[11] S. Garnerone, D. Abasto, S. Haas, and P. Zanardi, Phys. Rev. A **79,** 032302 (2009).
[12] C. De Grandi, A. Polkovnikov, and. A. W. Sandvik, Phys. Rev. B **84,** 224303 (2011).
[13] M. V. Berry, Proc. R. Soc. Lond. A **392,** 45 (1984).
[14] Y. Aharonov and D. Bohm, Phys. Rev. **115,** 485 (1959).
[15] M. Atala, M. Aidelsburger, J. T. Barreiro, D. Abanin, T. Kitagawa, E. Demler, and I. Bloch, Nature Physics **9,** 795 (2013).
[16] G. Sundaram abd Q. Niu, Phys. Rev. B **59,** 14915 (1999).
[17] K. Y. Bliokh, A. Niv, V. Kleiner, and E. Hasman, Nature Photonics, **2,** 748 (2008).
[18] J. Zak, Phys. Rev. Lett. **62,** 2747 (1989).
[19] M. Z. Hasan and C. L. Kane, Rev. Mod. Phys. **82,** 3045 (2010).
[20] M. Hafezi, S. Mittal, J. Fan, A. Migdall, and J. M. Taylor, Nature Photonics **7,** 1001 (2013).
[21] C.-Z. Chang *et al.*, Science **340,** 167 (2013).
[22] J. Anandan, Phys. Lett. A **133,** 171 (1988).
[23] P. San-Jose, G. Zarand, A. Shnirman, and G. Schön, Phys. Rev. Lett. **97,** 076803 (2006).
[24] Non-Abelian statistics and topological quantum information processing in 1D wire networks J. Alicea, Y. Oreg, G. Refael, F. von Oppen, and M.P. A. Fisher, Nature Physics **7**, 412 (2011).
[25] L. C. Venuti and P. Zanardi, Phys. Rev. Lett. **99,** 095701 (2007).
[26] P. W. Anderson, Phys. Rev. **109,** 1492 (1958).
[27] B. Kramer and A. MacKinnon, Rep. Prog. Phys. **56,** 1469-1564 (1993).
[28] M. A. Werner, A. Brataas, F. von Oppen, and G. Zarand, Phys. Rev. B **91,** 125418 (2015).
[29] E. Abrahams, P. W. Anderson, D. C. Licciardello, and T. V. Ramakrishnan, Phys. Rev. Lett. **42,** 673 (1979)
[30] A. MacKinnon and B. Kramer, Phys. Rev. Lett. **47,** 1546 (1981).
[31] K. Slevin and T. Ohtsuki, New J. Phys. **16,** 015012 (2014).
[32] K. Slevin and T. Ohtsuki, Phys. Rev. Lett. **78,** 4083 (1997).
[33] D. E. Khmel'nitskii and A. I. Larkin, Solid State Commun. **39,** 1069 (1981).
[34] G. Zaránd, C. P. Moca, and B. Jankó, Phys. Rev. Lett. **94,** 247202 (2005).
[35] F. Wegner, Nucl. Phys. B **270,** 1-9 (1986).
[36] X.-F. Wang, Z. Wang, G. Kotliar, and C. Castellani, Phys. Rev. Lett. **68,** 2504 (1992).
[37] M. Batsch, L. Schweitzer, I. Kh. Zharekeshev, and B. Kramer, Phys. Rev. Lett. **77,** 1552 (1996).
[38] J. T. Edwards and D. J. Thouless, J. Phys. C **5,** 807 (1972).
[39] D. J. Thouless, M. Kohmoto, M. P. Nightingale, and M. den Nijs, Phys. Rev. Lett. **49,** 405 (1982).
[40] Supplemental Material to this work.
[41] L. Ujfalusi and I. Varga, Phys. Rev. B **91,** 184206 (2015).
[42] K. G. Wilson, Rev. Mod. Phys. **47**, 773 (1975).
[43] C. M. Canali, Chaitali Basu, W. Stephan, and V. E. Kravtsov, Phys. Rev. B **54,** 1431 (1996).
[44] F. von Oppen, Phys. Rev. Lett. **73**, 798 (1994).
[45] F. von Oppen, Phys. Rev. E **51**, 2647 (1995).
[46] D. A. Greenwood, Proc. Phys. Soc. **71,** 585 (1958).
[47] T. Kawarabayashi, T. Ohtsuki, K. Slevin, and Y. Ono, Phys. Rev. Lett. **77,** 3593 (1996).
[48] A. Pal and D. A. Huse, Phys. Rev. B **82,** 174411 (2010).
[49] M. Filippone, P. W. Brouwer, J. Eisert, and F. von Oppen, Phys. Rev. B **94,** 201112(R) (2016).

Supplemental Material to "Universal Scaling Theory of the Boundary Geometric Tensor in Disordered Metals"

EXPLICIT FORMULAS FOR THE BOUNDARY GEOMETRIC TENSOR

In this section we derive explicit expressions for the quantum geometric tensor (QGT) [S1], used in our analysis. The Hamiltonian, Eq. (2) of the main text, is supplemented by twisted boundary conditions. In a finite system, this boundary condition appears through the hopping terms at the boundary: there electron operators outside the boundary ($\mathbf{r}'$) are replaced by phase shifted operators inside the boundary, $\mathbf{r} = \mathbf{r}' - \mathbf{n}L$, as

$$c_{\mathbf{r}'} = e^{i\mathbf{n}\cdot\boldsymbol{\phi}} c_{\mathbf{r}} \ , \tag{S.1}$$

with $\mathbf{n} = (n_x, n_y, n_z)$ appropriately chosen integers and $\boldsymbol{\phi} = (\phi_x, \phi_y, \phi_z)$ the boundary twists. We can restore the periodic boundary conditions by performing the gauge transformation,

$$\tilde{c}_{\mathbf{r}} = e^{-\frac{i}{L}\mathbf{r}\cdot\boldsymbol{\phi}} c_{\mathbf{r}} \ , \tag{S.2}$$

In terms of these, the Hamiltonian becomes

$$\hat{H} = \sum_{\mathbf{r}} V(\mathbf{r}) \tilde{c}^{\dagger}_{\mathbf{r}} \tilde{c}_{\mathbf{r}} - \sum_{\langle \mathbf{r},\mathbf{r}' \rangle} \left(t_{\mathbf{r}\mathbf{r}'} \ e^{\frac{i}{L}(\mathbf{r}-\mathbf{r}')\cdot\boldsymbol{\phi}} \ \tilde{c}^{\dagger}_{\mathbf{r}} \tilde{c}_{\mathbf{r}'} + h.c. \right) \ . \tag{S.3}$$

To express the QGT, we need the derivatives

$$\frac{\partial \hat{H}}{\partial \phi_k} = - \sum_{\langle \mathbf{r},\mathbf{r}' \rangle} \left(\frac{i}{L} (r_k - r'_k) t_{\mathbf{r}\mathbf{r}'} \ e^{\frac{i}{L}(\mathbf{r}-\mathbf{r}')\cdot\boldsymbol{\phi}} \ \tilde{c}^{\dagger}_{\mathbf{r}} \tilde{c}_{\mathbf{r}'} + h.c. \right) \ . \tag{S.4}$$

Expanding then $\hat{H}(\boldsymbol{\phi} + d\boldsymbol{\phi}) = \hat{H}(\boldsymbol{\phi}) + d\boldsymbol{\phi} \cdot \frac{\partial \hat{H}}{\partial \boldsymbol{\phi}} + \dots$ and performing first order perturbation theory in $d\boldsymbol{\phi}$ we obtain

$$Q_{ij}(\alpha) = \sum_{\beta \neq \alpha} \frac{\langle \alpha \rangle \, \partial \hat{H}/\partial \phi_i \, |\beta\rangle \, \langle \beta \rangle \, \partial \hat{H}/\partial \phi_j \, |\alpha\rangle}{(E_\alpha - E_\beta)^2} \ . \tag{S.5}$$

THE QUANTUM GEOMETRIC TENSOR AND THE THOULESS NUMBER

The Thouless number [S2], defined as the disorder averaged absolute curvature of the single particle energies at energy E, divided by the mean level spacing Δ at E, is a commonly used indicator in the field of Anderson transitions,

$$\mathcal{C}_T = \frac{\pi}{\Delta} \left\langle \left| \frac{\partial^2 E_\alpha}{\partial \phi_x^2} \right| \right\rangle_{E_\alpha = E} \tag{S.6}$$

Similar to the parameter g_{typ} (see (6) in the main text), it is a function of energy, system size, disorder strength, and magnetic field. As argued in Ref. S2, and numerically demonstrated in Ref. S3, the Thouless number (S.6) measures the dimensionless DC conductance of a finite system.

Fig. S1 shows the connection between the Thouless number and the parameter $g_{\text{typ}} \sim \operatorname{tr} Q$. We observe an approximately linear connection between the two parameters; however, a significant difference appears in the dependence of $\mathcal{C}_T$ on g_{typ} in the presence, or absence of a strong enough external magnetic field. Nevertheless, the one-to-one connection between g_{typ} and $\mathcal{C}_T$ in the universal limits implies analogous one parameter scaling properties for both $\mathcal{C}_T$ and g_{typ}. Using g_{typ} instead of the Thouless number is therefore a legitimate choice.

FINITE SIZE SCALING OF THE QGT IN A HOMOGENEOUS MAGNETIC FIELD

As stated in the main text, one cannot observe the orthogonal-unitary crossover in homogeneous magnetic fields, because there is at least one flux quantum pierced through a system on a torus. As shown in Fig. S2, the extracted

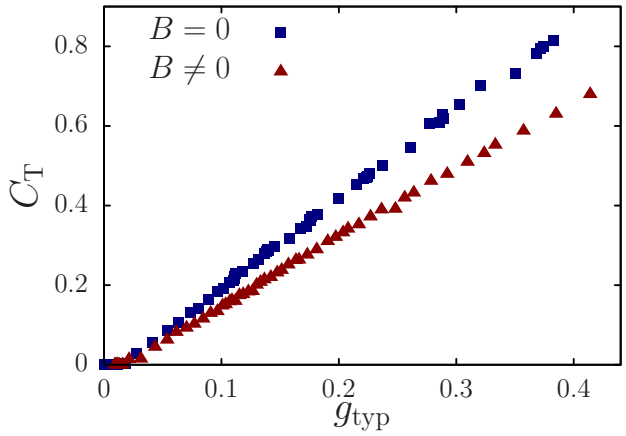

FIG. S1. The Thouless number $\mathcal{C}_T$ as a function of the parameter $g_{\rm typ}$: the precise relation between these two parameters depends on the universality class. In case of a homogeneous or strong random magnetic field, one finds the same $\mathcal{C}_T(g_{\rm typ})$ function, which is clearly different from the one obtained for $B = 0$.

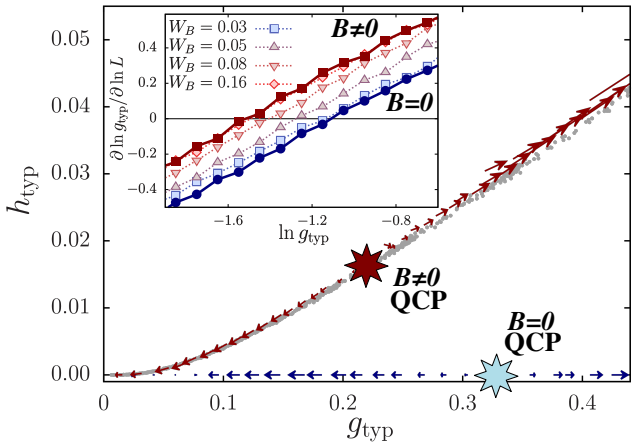

FIG. S2. Finite size scaling of the parameters $g_{\rm typ}$ and $h_{\rm typ}$ in homogeneous (red arrows) and zero (blue arrows) magnetic fields. The renormalization group trajectories fall on distinct one parameter curves in the two cases. The quantum critical points of the $B = 0$ (orthogonal) and $B \neq 0$ (unitary) universality classes are denoted by light blue and dark red stars, respectively. The flow in homogeneous field is calculated using a field strength of $B = \Phi_0/9$, while the system size is increased from $L = 9$ to $L = 12$. The gray dots show the data in the smallest simulated homogeneous field, $B = \Phi_0/196$, with $L = 14$. *Inset:* Universal scaling functions $\beta = \frac{\partial \ln g_{\rm typ}}{\partial \ln L}$ for $B = 0$ (dark blue circles) and $B \neq 0$ (dark red squares). Light symbols show the naively calculated β-functions in weak random magnetic fields, while the system size is increased from $L_1 = 8$ to $L_2 = 14$. These non-universal curves are close to the orthogonal scaling function for the weakest fields but they approach the unitary scaling function as we increase the strength of the random field.

RG trajectories fall on two distinct lines in the $\{g_{\rm typ}, h_{\rm typ}\}$ plane for $B = 0$ and $B \neq 0$. Even in the smallest magnetic field we could simulate ($B = \Phi_0/196$ in the units of flux/cell, and $L = 14$), the data points fall on the same line corresponding to the $B \neq 0$ universality class, and we cannot observe any trace of the unitary-orthogonal crossover in homogeneous fields. The positions of $B \neq 0$ trajectories and critical points in Fig. S2 coincide with the ones in Fig. 1 of the main text computed in a random field. This agreement strongly supports that models with homogeneous and strong random fields fall in the same universality class.

The inset of Fig. S2 shows the one parameter β-functions ($\beta(g_{\rm typ}) = \partial \ln g_{\rm typ}/\partial \ln L$) in the two universality classes. In addition we show the naively calculated β-functions in weak random magnetic fields, obtained by calculating numerically the derivative $\partial \ln g_{\rm typ}/\partial \ln L$ by increasing the system size from $L = 8$ to $L = 14$. We find a "motion" of these naive curves from the $B = 0$ to the $B \neq 0$ universal β functions upon increasing the size of the random field.

This continuous crossover demonstrates the failure of the one parameter scaling theory in weak random fields: there is necessarily a second relevant scaling variable at the orthogonal critical point that describes the crossover.

DETAILS OF FITTING THE CRITICAL POINTS AND EXPONENTS

To extract the critical parameters of the fixed points in the RG flow of Fig. 1. we rewrite Eq. (6) into a vectorial form and then linearize the equation around the fixed points to get

$$\frac{\partial}{\partial \ln L}\begin{pmatrix} g_{\rm typ} \\ h_{typ}\end{pmatrix} = \begin{pmatrix} M_{gg} & M_{gh} \\ M_{hg} & M_{hh}\end{pmatrix}\left[\begin{pmatrix} g_{\rm typ} \\ h_{typ}\end{pmatrix} - \begin{pmatrix} g^*_{\rm typ} \\ h^*_{typ}\end{pmatrix}\right] = \begin{pmatrix} M_{gg} & M_{gh} \\ M_{hg} & M_{hh}\end{pmatrix}\begin{pmatrix} g_{\rm typ} \\ h_{typ}\end{pmatrix} - \begin{pmatrix} b_g \\ b_h\end{pmatrix} . \qquad \text{(S.7)}$$

Here $g^*_{\rm typ}$ and $h^*_{\rm typ}$ denote the coordinates of the corresponding fixed point, while the matrix $\underline{\underline{M}}$ drives the linearized flow. In (S.7) we introduced the vector $\begin{pmatrix} b_g \\ b_h\end{pmatrix} = \underline{\underline{M}}\begin{pmatrix} g^*_{\rm typ} \\ h^*_{typ}\end{pmatrix}$ to transform (S.7) into a form where the dependence on the parameters $\underline{\underline{M}}$, b_g, and b_h is linear. We can then use the machinery of multivariate linear regression to extract $\underline{\underline{M}}$ and $\underline{b}$ [S4]. The coordinates of the fixed point are then expressed as $\begin{pmatrix} g^*_{\rm typ} \\ h^*_{\rm typ}\end{pmatrix} = \underline{\underline{M}}^{-1}\underline{b}$, while the critical exponents of the fixed point are the eigenvalues of $\underline{\underline{M}}$. At the orthogonal ($B = 0$) fixed point, one can further exploit the fact that in the absence of the magnetic field the parameter $h_{\rm typ}$ vanishes, and thereby reduce the number of fitting parameters from 6 to 4.

THE CRITICAL DISTRIBUTION OF $g(\alpha)$

We have determined numerically the critical distribution of the trace of the geometric tensor, $g(\alpha) = \mathrm{tr}\{Q_\alpha\}$, both at the orthogonal and at the unitary critical points. The observed $p(g)$ functions, shown in Fig. S3, are similar at the two critical points, but exhibit important differences, too (see panels (a) and (b) of Fig. S3). At both critical points, $p(g)$ displays power-law tails $\sim g^{-\eta}$ at large g. However, while at the unitary critical point we observe an exponent $\eta \approx 2.5$, at the orthogonal critical point $\eta \approx 2$ seems to emerge. Both exponents are consistent with the expression, $\eta = \beta/2 + 3/2$, with $\beta = 1$ and $\beta = 2$ the usual parameters classifying the orthogonal and unitary universality classes, respectively. The exponent η is clearly different from the exponent $\tilde{\eta} = 2 + \beta$ characterizing the distribution of the Thouless curvatures, $c_\alpha \equiv \pi\,|\partial^2_\phi E_\alpha|/\Delta$, defined as the dimensionless level curvature, with Δ referring to the typical level spacing (see red data points in Fig. S3).

The observed exponent $\eta = \beta/2 + 3/2$ follows from the expression Eq. (S.5) under the assumption that the sum is dominated by a single term with an anomalously small level separation, $s \equiv |E_\alpha - E_{\beta=\alpha+1}| \ll \Delta$. By assuming furthermore that small level separations obey Wigner-Dyson statics even at the critical point, $p(s) \propto s^\beta$, we arrive

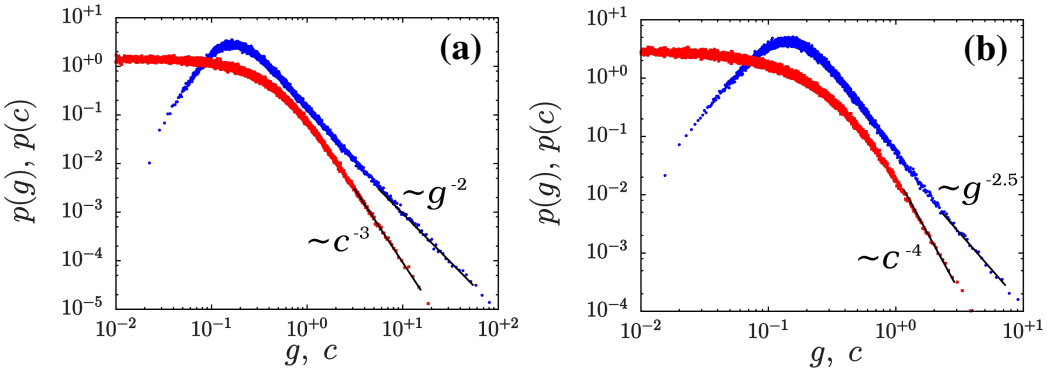

FIG. S3. **(a)-(b)** Critical distributions of the trace of the geometric tensor, $g(\alpha) = \mathrm{tr}\{Q_\alpha\}$, and the dimensionless level curvature $c_\alpha = \pi\,|\partial^2 E_\alpha/\partial\phi^2|/\Delta$ at the orthogonal ($B = 0$) and unitary ($B \neq 0$) critical points, respectively. Blue symbols represent the distribution $p(g)$, while red symbols represent $p(c)$. The observed exponents are consistent with the predictions of random-matrix theory.

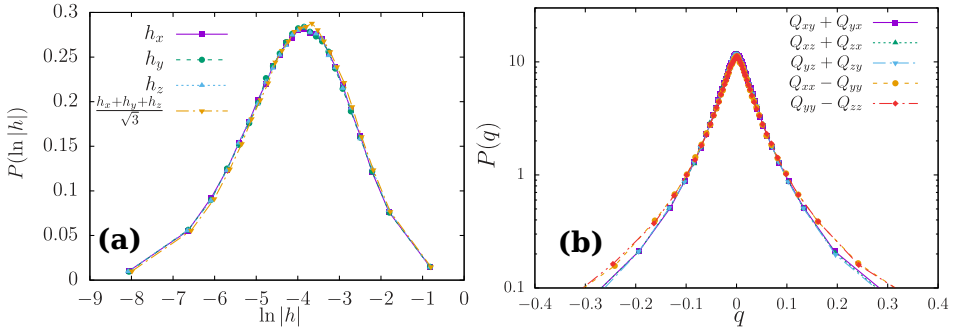

FIG. S4. (a) Probability density function of $\ln|h_i|$ and $\ln(|h_x+h_y+h_z|/\sqrt{3})$. In the latter case the distribution slightly distorts, that is an evidence for the breaking of the full rotational symmetry. (b) Probability density functions of $Q_{xy}+Q_{yx}$, $Q_{xz}+Q_{zx}$, $Q_{yz}+Q_{zy}$, $Q_{xx}-Q_{yy}$, and $Q_{yy}-Q_{zz}$. The distribution slightly differs for the latter two case, that is again an evidence for breaking of the full rotational symmetry.

immediately at the prediction, $p(g) \propto g^{-(\beta/2+3/2)}$ for large g. Similar arguments imply a fall-off $p(c) \propto c^{-(\beta+2)}$ for the distribution of the level dependent Thouless curvature, c_α [S5–S7].

DETAILED ISOTROPY ANALYSIS AT THE $B \neq 0$ (UNITARY) FIXED POINT

As stated in the main text, the unitary ($B \neq 0$) critical point has a surprising isotropy: at the critical point the direction of a homogeneous magnetic field appears to be irrelevant. In addition, the joint distribution of the generalized parameters h_k seems to have full rotational symmetry (O(3)) at first sight (see Fig. 2 in the main text). Here we show in more details that, according to our data, the full O(3) symmetry is slightly broken and lowered to the discrete octahedral symmetry, interpreted as an effect of the cubic shape of our system.

The QGT, as defined in Eq. (1), follows the usual transformation laws of tensors under rotations: i.e. if one transforms the twist phases $\underline{\phi} = (\phi_x, \phi_y, \phi_z)$ with an orthogonal transformation $\underline{\phi} \to \underline{\underline{O}}\,\underline{\phi}$, then the QGT transforms as

$$\underline{\underline{Q}} \to \underline{\underline{O}}\,\underline{\underline{Q}}\,\underline{\underline{O}}^T . \tag{S.8}$$

At the critical points the QGT is a random variable, with a probability density function $P\left(\underline{\underline{Q}}\right)$. The transformation $\underline{\underline{O}}$ is a symmetry of the distribution, if

$$P\left(\underline{\underline{Q}}\right) \equiv P\left(\underline{\underline{O}}\,\underline{\underline{Q}}\,\underline{\underline{O}}^T\right) \tag{S.9}$$

for every $\underline{\underline{Q}}$.

The parameters h_k introduced in Eq. (11) parametrize the antisymmetric part of the tensor. As a result, these parameters follow the usual transformation laws of (axial-)vectors under orthogonal transformations,

$$\underline{h}' = \det(\underline{\underline{O}})\,\underline{\underline{O}}\,\underline{h} . \tag{S.10}$$

Consequently, if the distribution of $\underline{\underline{Q}}$ had full $O(3)$ symmetry, the joint distribution of parameters h_k would be spherically symmetric. One consequence of such a high symmetry on the marginal distributions would be the relations

$$P(h_i) \stackrel{?}{=} P(h_j) \stackrel{?}{=} P\left((h_i+h_j+h_k)/\sqrt{3}\right) , \tag{S.11}$$

with $i \neq j \neq k$. To test this symmetry, we first determine the typical magnitudes in the critical point, $(h_k)_{\text{typ}} = 0.01683(13)$, and $\left((h_i+h_j+h_k)/\sqrt{3}\right)_{\text{typ}} = 0.01769(11)$. This slight change is also directly visible in the probability density function. The distribution of $\ln|h|$ is shown in Fig. S4, and only a slight shift is visible in the case of $(h_i+h_j+h_k)/\sqrt{3}$; however, the distortion of the distribution is hardly visible.

The breaking of the rotational symmetry is stronger in the symmetric part of the QGT. If the tensor was O(3) symmetric, the following combinations would be equivalent,

$$P\left(Q_{xy}+Q_{yx}\right),\ P\left(Q_{yz}+Q_{zy}\right),\ P\left(Q_{zx}+Q_{xz}\right),\ P\left(Q_{xx}-Q_{yy}\right),\ \text{and}\ P\left(Q_{yy}-Q_{zz}\right)\ . \tag{S.12}$$

As shown in panel (b) of Fig. S4, for $Q_{xx} - Q_{yy}$ and $Q_{yy} - Q_{zz}$ the distributions are significantly distorted. The separation of the diagonal and off-diagonal combinations can be explained as an effect of the lowering of the full O(3) symmetry to the discrete octahedral (O_h) symmetry group.

We believe that in an infinite system the critical point should have full isotropy, i.e. the microscopic direction of the lattice gets irrelevant. In a finite system, however, the critical state extends over the whole system, and it is therefore unavoidably affected by the boundaries.

[S1] M. Kolodrubetz, D. Sels, P. Mehta, and A. Polkovnikov, Physics Reports **697,** 1 (2017).
[S2] J. T. Edwards and D. J. Thouless, J. Phys. C **5,** 807 (1972).
[S3] D. Braun, E. Hofstetter, A. MacKinnon, and G. Montambaux, Phys. Rev. B **55**, 7557 (1997).
[S4] R. Christensen, Advanced Linear Modeling (Springer-Verlag, New York, 2001), Second Edition.
[S5] F. von Oppen, Phys. Rev. Lett. **73,** 798 (1994).
[S6] F. von Oppen, Phys. Rev. E **51**, 2647 (1995).
[S7] C. M. Canali, Chaitali Basu, W. Stephan, and V. E. Kravtsov, Phys. Rev. B **54,** 1431 (1996).